
Deepfake Caricatures: Amplifying attention to artifacts increases deepfake detection by humans and machines

Camilo Fosco*
MIT
camilolu@mit.edu

Emilie Josephts*
MIT
ejosephts@mit.edu

Alex Andonian
MIT
andonian@mit.edu

Aude Oliva
MIT
oliva@mit.edu

1 Link to view Caricatures in Video Form

The effect of our caricatures is best experienced in video form. We provide a compilation of examples in the supplementary mp4 file *caricature_applied_on_fake_vids.mp4*. In the clip, we show the impact on the Caricature generation process on deepfakes. The artifacts are amplified and the video is generally distorted. We additionally provide an anonymized web gallery, *gallery.html*, that allows for easy visualization of several additional examples. Once the *gallery.html* file is extracted from the provided zip, along with its accompanying videos, double click on the html file to view it on your browser.

2 Video Selection for Human Artifact Annotations

2.1 Selecting challenging deepfakes according to humans.

Selecting target videos for our human artifact annotations poses a challenge: we would like videos to be hard to detect as fakes by humans, to ensure that our artifacts are a) non-trivial, and b) capture the subtleties of well-functioning face alteration techniques. To facilitate this selection, we formulated a crowd sourced experiment to find fake videos that are relatively difficult to detect as fake, without scrutiny.

We randomly selected 1000 video pairs (1000 real, 1000 fake) from the Deepfake Detection Challenge Dataset (4) and used FaceNet (18) to crop the face regions, resulting in videos of 360×360 pixels. These 1000 were randomly divided into sets of 100, and each set received 10 responses. Participants were instructed to maintain their fixation at a center cross while a pair of videos were presented, one on the left and one on the right (Figure 1). One of those videos was fake, while the other one was real. Participants were asked to select which video was more likely to be fake by pressing a left or right keyboard key. At the start of the experiment, people had the possibility to adjust the distance between the videos (left and right videos were always at the same distance from the center). To help with the adjustment, the following instructions were given “The videos should not be too close to disturb you from fixating at the center, and not too far away to notably reduce your ability to distinguish them. Find the distance that feels more comfortable to you.” After every 10 videos shown to users, users took a quick break and then had 3 seconds to refocus their attention on the fixation cross before examining the next set of videos. Participants were asked to report whenever their gaze shifted towards either side of the videos, in which case the trial was discarded.

We computed video difficulty by averaging the responses over videos. Based on those responses, we selected 500 fake videos that were closest to having a 50% recognition rate, which indicated that human detection performance was close to chance. Those videos were considered “hard to detect”.

*Equal contribution

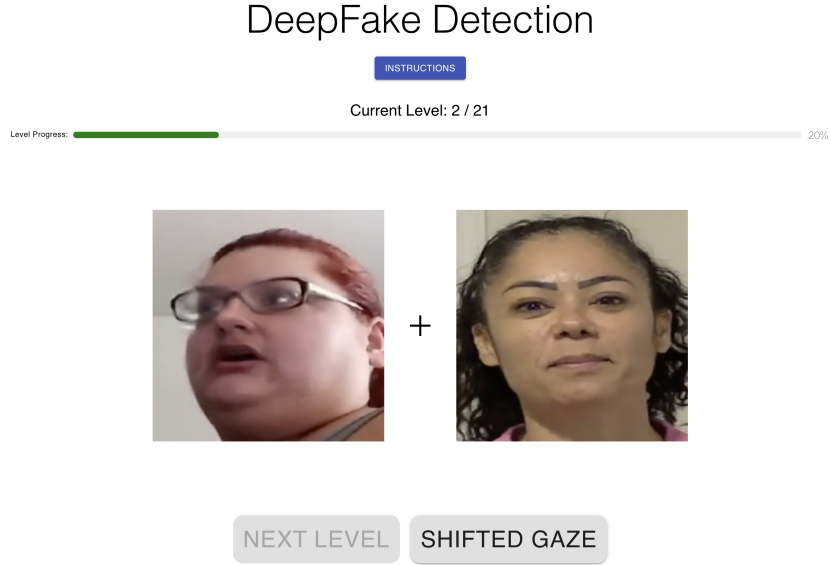


Figure 1: Screenshot of the interface used to collect human detection difficulty. Humans were tasked with indicating which of the two videos was fake without shifting their gaze from the cross.

2.2 Selecting challenging fakes according to models.

We would additionally like to represent the distribution of hard fakes for models, and collect human artifact maps on these fakes to ensure our distribution of maps covers the space of challenging artifacts. For this, we selected 500 fake videos from our DFDCp training split that minimized the "fake" classification confidence (output of the softmax) of an Xception network trained on FF++, while not being a duplicate of the 500 videos selected through our human experiment.

3 Video artifact annotations

3.1 Methods

Videos were annotated in an online task that used a paintbrush interface. Participants were instructed to paint over the regions that were most informative about whether a video was fake. Videos were paused during painting, and the interface contained a separate visualization of where the participant has painted, so they could keep track of their annotations.

3.2 Qualitative results

In total we collected over 11K annotations for 1000 videos. On average, each video had annotations from 22.6 participants, resulting in 4.1K sample points per video. For each video clip, we aggregated all annotation data and generated one 3D attention map: An anisotropic Gaussian kernel of size $(c \cdot s, c \cdot s, 6)$ in x,y and time dimensions was first applied. c is set to a constant 20px and s corresponds to the brush size. We normalize the attention map of each time frame to sum to one.

Humans tend to annotate areas of the face that are near the eyes or mouth, which are more salient facial features. Our model picks up on these features as well as other areas that are indicative of doctoring. For example, there is attention to inflection regions of the face, such as the jawline or near the hairline. Humans also gravitate towards inconsistencies around the seams generated by the face swapping pipeline, as well as flickering artifacts generated by tracking errors during the deepfake process.

4 Model Loss

We utilize a dual loss to train our prediction and caricature generation network. The fake / real output of our classification module is supervised with a typical binary cross-entropy loss L_{BCE} :

$$L_{BCE} = -\frac{1}{N} \sum_{i=1}^N y_i \cdot \log(\bar{y}_i) + (1 - y_i) \cdot \log(1 - \bar{y}_i)$$

Where N is the number of elements in our dataset.

Additionally, we impose another loss on the system: a correlation loss L_{human} ensures that the output of the artifact attention module reproduces the ground truth human maps. This loss is composed of a KL-divergence component, a Pearson Correlation Coefficient component, and an L1 loss component, all weighted by specific factors determined experimentally. The loss takes the following form:

$$L_{human} = \alpha L_{KL} + \beta L_{CC} + \gamma L^1$$

Let p and q be the predict and ground truth maps respectively, M the total number of pixels in the map, and $\epsilon = 1e - 7$ to avoid numerical issues. We have:

$$L_{KL}(p, q) = \sum_i q_i \log \left(\epsilon + \frac{q_i}{\epsilon + p_i} \right)$$

$$L_{CC}(p, q) = \frac{\sigma(p, q)}{\sigma(p) \cdot \sigma(q)}$$

$$L^1(p, q) = \frac{1}{M} \sum_i |p_i - q_i|$$

These losses are computed element-by-element and averaged over a minibatch during training. We perform a simple grid search to determine adequate loss parameters and converge to the following values: $\alpha = 1$, $\beta = -0.5$, $\gamma = 1$. Note that β is negative to ensure the correlation coefficient is maximized.

The total loss L of our model is $L = L_{BCE} + L_{human}$.

5 Details of benchmarks and baselines for model evaluation

5.1 Datasets

We evaluated models on four benchmarks:

FaceForensics++ (FF++) (16), which contains more than 1.8M images generated from 5000 YouTube videos. It features four different facial manipulation methods, which are Deepfake (3), Face2Face (22), FaceSwap (9) and NeuralTextures (21), and covers a large variation in video resolution ranging from 1080p to 480p. We use 8151 images for training, 280 images for validation, and 280 for testing. To ensure fair comparisons with (6) and others, we use the first 270 frames of each training video and the first 110 frames for each validation video.

The Deepfake Detection Challenge Dataset (DFDCp) (4). We use the preview version of this dataset, which contains 3754 fakes and 1460 real videos. Two facial modification methods were used to generate the fake videos, however, no specific labels were given regarding the generation method. In this work, we report performance on the publicly available validation set of 400 labeled videos.

Celeb-DF v2 (13) dataset provides 5639 synthesized fake videos of celebrities generated from 590 real videos. Based on a tandem auto-encoder architecture, a video synthesis method that puts special emphasis on reducing visual artifacts was used to generate high quality fake videos. In our experiment, we split the dataset into a training set of 6011 videos, and a validation set of 518 videos.

DeeperForensics (DFo) (13), which contains 10000 fake videos obtained by taking 1000 real videos from FF++, and swapping in faces of 100 new paid actors.

FaceShifter (FShifter) (10), which also consists of 10000 fake videos generated by doctoring the real videos from FF++.

Video Standardization Videos from the different datasets under study were preprocessed to bring them into a standard configuration. All datasets were downloaded at full resolution, except FaceForensics++, which was downloaded in the provided *c23* compressed format to avoid large storage costs. We performed multi-person face extraction on all videos using a pretrained PyTorch implementation of FaceNet(18), with a minimum face size of 50 pixels and a face margin size of 100 pixels. For frames without a detected face, bounding box coordinates were produced via linear interpolation of the next available neighboring bounding boxes. To avoid abrupt motion artifacts (e.g. jittering) from face extraction, the 4 corner coordinates of the detected bounding boxes were temporally smoothed using hanning smoothing with a window size equal to 20% the video length. These face frames were resized to 360×360 pixels and saved as an MP4 file.

5.2 Baseline Models

Clip-based ResNet: Building on features learned from ImageNet, the inflation of pretrained 2D kernels into 3D has shown significant improvement on video-based tasks (2; 7; 23). As a baseline of 3D CNN, We use a 3D ResNet model where the 3D kernels are inflated from ResNet18 pretrained on the Kinetics dataset (1).

XceptionNet, which was trained on the FaceForensics++ dataset.

Face X-ray, which attends to the seams in face-swapping to make its predictions. We use existing performance values from (6) for the FF++ trained results, and evaluate an HRNet-W48 trained on synthetic blended images in conjunction with FF++ videos for our DFDCp results.

The *CNN-GRU* from (17), where we train a DenseNet-161 followed by a GRU on FF++ to evaluate on DFDCp, and report existing performance values for FF++.

The *Multi-task* model from (15). We report existing numbers from (6) and retrain using the publicly available implementation.

DSP-FWA, a model that tries to detect face warping artifacts. We evaluate the publicly available pretrained model for FF++, and train a ResNet50 with the pyramidal setup introduced in (12) for DFDCp.

The *Two-branch* model from (14). We report existing numbers for CelebDFv2 evaluation, and retrain on the rest.

The *Multi-attention* model from (24). We report the values from the existing paper, and retrain following the setup in the paper on FF++ for DFDCp results.

The Lip Forensics approach from (6). We use their publicly available values for our main tables.

6 User study: Extended Methods

6.1 Study 1: How do Caricatures Compare to text-based indicators

Stimuli. Stimuli consisted of 50 real and 50 fake videos selected from DFDC. The 50 fake videos were high-quality deepfakes, which were difficult for human participants to detect. These were selected by running a separate pilot deepfake detection task on a larger subset of the DFDC, and selecting 50 videos with detection rates between 30% and 10%, to have a range of difficulty. We focused on difficult deepfakes because this provides the best test-case of how convincing a visual indicator is; users would not need to rely on a visual indicator if they can see the artifacts for themselves.

Behavioral Task. The behavioral task was a simple 2-alternative forced choice task. Users were shown one video at a time, and were asked to assess whether the video was real or fake. There were three condition, presented in a between-subjects manner. In the unaided detection condition, real and fake videos were presented as-is, with no further modifications. In the text-based indicator condition, a badge was added to the top-left corner of all fake videos which said "video modified by AI" in bold white letters on a semi-opaque bright turquoise background. In the caricature condition, the Deepfake Caricature transformation was applied to all fake videos prior to presentation.

Participants. Participants consisted of 90 workers on Prolific.com. Participation was restricted to individuals over the age of eighteen, located in the US, with approval ratings over 90%. Participants were recruited and compensated according to procedure approved by the [University's] Committee on the Use of Humans as Experimental Subjects. Participants were paid according to an hourly rate of \$11.25 per hour.

Analysis. Hit rates were calculated for each subject, and averaged across subjects for each condition. Hit rates were compared across conditions using planned t-tests.

6.2 Study 2: What range of conditions are Caricatures effective in

Stimuli. Stimuli consisted of 400 videos selected from DFDCp (4). Half of the videos contained real, unaltered faces, while the other half contained deepfake faces. Videos were randomly selected, then deepfakes with obvious artifacts were discarded. All videos were subjected to the standardization procedure described above, and were presented at a resolution of 300x300 pixels. These 200 fake videos made up the stimuli for the "standard deepfake" condition. These videos were then passed through CariNet to receive modulation from the Caricature Creation Module, yielding stimuli for the "Caricature" condition.

Behavioral Task. Participants performed a two-alternative forced choice detection task. They were shown one video at a time and were asked to indicate if the video was real or fake by using the mouse to click on buttons labeled "Real" and "Fake". Prior to the tasks, participants were shown instructions which included 3 example deepfakes, to inform them about what a fake video looks like.

Each task session contained 100 videos, divided into 5 blocks of 20 videos with breaks in between. Videos could be presented at 6 different presentation durations: 300ms, 500ms, 1000ms, 3000ms and 5000ms. Each trial started with a 3 second countdown. In addition, each block contained one compliance check, and one engagement probe. Compliance checks consisted of real or fake videos (not included in the experimental set) with the text "THIS IS AN ATTENTION CHECK, PLEASE CLICK REAL" written across the video in light grey font. These trials were included to provide an objective basis by which to exclude low-performing participants (see Analysis section below). Engagement probes consisted of deepfakes (not included in the experimental set) containing extremely obvious artifacts, such as large patches of noise covering the face. These trials were included to provide an on-line measure of participants attentiveness. We reasoned that while highly-engaged participants would succeed on all of these trials, medium to low-engagement participants would miss some proportion of them.

Trials were divided into experimental sessions (or "HITS") of 100 trials. Trials were assigned to HITs pseudo randomly, with the exception that no fake or caricature could be shown twice in the same HIT. Data were collected for 19 HITs of randomly selected videos, leading to an average of 72 videos per presentation time for both standard fakes and caricatures. We collected 10 participants per each HIT.

Participants. Participants consisted of 170 workers on Amazon Mechanical Turk. Participation was restricted to individuals over the age of eighteen, located in the US, with approval ratings over 99%. Participants were recruited and compensated according to procedure approved by the [University’s] Committee on the Use of Humans as Experimental Subjects. Participants were paid according to an hourly rate of \$11.25 per hour.

Analysis. We collected 10 judgments per video per condition. This number was selected after a power analysis (performed on a pilot set of 100 HITs), which suggested that 6 responses was sufficient to obtain stable estimates of the mean detectability of a given video.

Our primary analysis was to examine the difference in correct detection rates between the standard deepfake condition and the caricature condition, both pooling over presentation times and for each presentation time individually. As such, we pre-registered an ANOVA analysis to test for a main effect of condition on accuracy, with the hypothesis that correct detection would be higher in the caricature than standard deepfake condition. We additionally hypothesized that overall detection (pooling across conditions) would be higher for longer presentation times (main effect of presentation time), and that the difference between standard and caricature deepfakes would increase with higher presentation time (significant interaction), although these analyses were orthogonal to the main question of this experiment. We also planned further comparisons between the standard and caricature conditions for each time point individually. We pre-registered individual unpaired t-tests at a conservative alpha level of $p = 0.0083$ (Bonferroni correction for performing 6 individual t-tests, one per time point). To ensure quality data for this analysis, we excluded any sessions where participants used only one key, or failed three or more compliance checks. These trimming and analysis procedures were developed in an initial pilot dataset of 100 HITs, then applied in the experimental dataset (i.e. they were pre-registered). We elected to use the conservative Bonferroni correction even though these were a-priori analyses because this experiment had high enough power to detect effects even at conservative thresholds, and applying this threshold would reduce the chance of Type I error.

We also performed a second analysis to examine the effects of condition across levels of participant attentiveness. We divided HITs into participant engagement bins based on the number of engagement probes that were successfully detected throughout the HIT. As the dependent measure, we subtracted the correct detection rate in the standard condition from the caricature condition, to get a measure of the relative benefit of the caricature condition, and tested whether this difference was greater than 0 using a one-sided one-sample t-test at an alpha level of $p = 0.05$. We used a traditional rather than conservative p values because some conditions were likely to contain a low number of trials, and thus have lower power. Statistics were only carried out for conditions containing 10 or more datapoints. This analysis used all experimental sessions.

6.3 Complete statistical reporting

Analysis 1: ANOVA testing for an effect of condition

Effect	SS	df	F	p
Condition	2.17	4.0	16.46	3.13e-13
Presentation time	2.43	5.0	14.75	3.50e-14
Interaction	6.15	20.0	9.32	3.98e-20
Residual	54.79	1661.0	-	-

Table 1: ANOVA testing for an effect of condition.

Analysis 2: planned comparisons of detectability difference between standard fake and caricatures for each timepoint.

Timepoint	300ms	500ms	1000ms	3000ms	5000ms
df	155	160	159	129	172
t	4.58	7.97	9.11	11.23	12.86
p	9.2e-6	2.9e-13	3.1e-17	7.7e-21	5.9e-27

Table 2: Planned comparisons of detectability difference between standard fake and caricatures for each timepoint.

Analysis 3: Significance of the difference between standard fake and caricatures for each level of participant engagement.

Engagement	0.2	0.4	0.6	0.8	1.0
df	9	18	20	58	76
t	2.63	1.73	6.27	9.82	15.64
p	0.015	0.051	2.5e-06	3.6e-14	1.3e-25

Table 3: Significance of the difference between standard fake and caricatures for each level of participant engagement.

7 Results including the DFDCp-trained Artifact Attention Module

In the paper, we reported the results from a model with a FF++-trained Artifact Attention Module to ensure fair comparisons with prior work. Our DFDCp-trained model had similar performance, but did not perform with the same consistency as the FF++ trained model. We report the values here for completeness.

Model	CelebDFv2	DFDCp	FShifter	DFo	Overall
Xception (16)	73.7	65.7	72.0	84.5	75.3
Face X-ray (11)	79.5	62.1	92.8	86.8	81.2
CNN-GRU (17)	69.8	63.7	80.8	74.1	73.4
Multi-task (15)	75.7	63.9	66.0	77.7	71.9
DSP-FWA (12)	69.5	64.5	65.5	50.2	63.1
Two-branch (14)	73.4	64.0	-	-	-
Multi-attention (24)	67.4	67.1	-	-	-
LipForensics (24)	82.4	70.0	97.1	97.6	86.8
FTCN (25)	86.9	74.0	98.8	98.8	-
DCL (20)	82.3	<u>76.7</u>	92.4	97.1	-
RF (5)	86.9	75.9	99.7	<u>99.3</u>	-
S-B (19)	93.2	72.4	-	-	-
X+PCC (8)	54.9	62.7	-	-	-
CariNet DFDCp (ours)	<u>87.6</u>	77.1	<u>98.9</u>	99.3	-

Table 4: Detection performance results on unseen datasets.

Method	Train on remaining				Avg
	DF	FS	F2F	NT	
Xception (16)	93.9	51.2	86.8	79.7	77.9
CNN-GRU (17)	97.6	47.6	85.8	86.6	79.4
Face X-ray (11)	99.5	93.2	94.5	92.5	94.9
LipForensics (6)	99.7	90.1	99.7	99.1	99.5
CariNet DFDCp (ours)	99.9	99.9	99.8	99.4	99.8

Table 5: Generalization to unseen manipulations.

Method	Clean	Cont.	Noise	Blur	Pixel
Xception	99.8	98.6	53.8	60.2	74.2
CNN-GRU	99.9	98.8	47.9	71.5	86.5
Face X-ray	99.8	88.5	49.8	63.8	88.6
LipForensics	99.9	99.6	73.8	96.1	95.6
CariNet DFDCp	99.9	99.9	78.3	93.3	97.5

Table 6: **Generalization performance over unseen perturbations.**

References

- [1] J. Carreira, E. Noland, C. Hillier, and A. Zisserman. A short note on the kinetics-700 human action dataset. *arXiv preprint arXiv:1907.06987*, 2019.
- [2] J. Carreira and A. Zisserman. Quo vadis, action recognition? a new model and the kinetics dataset. In *proceedings of the IEEE Conference on Computer Vision and Pattern Recognition*, pages 6299–6308, 2017.
- [3] D. Deepfake. <https://github.com/deepfakes/faceswap>, 2020.
- [4] B. Dolhansky, R. Howes, B. Pflaum, N. Baram, and C. C. Ferrer. The deepfake detection challenge (dfdc) preview dataset. *arXiv preprint arXiv:1910.08854*, 2019.
- [5] A. Haliassos, R. Mira, S. Petridis, and M. Pantic. Leveraging real talking faces via self-supervision for robust forgery detection. In *Proceedings of the IEEE/CVF Conference on Computer Vision and Pattern Recognition*, pages 14950–14962, 2022.
- [6] A. Haliassos, K. Vougioukas, S. Petridis, and M. Pantic. Lips don’t lie: A generalisable and robust approach to face forgery detection. In *Proceedings of the IEEE/CVF Conference on Computer Vision and Pattern Recognition*, pages 5039–5049, 2021.
- [7] K. Hara, H. Kataoka, and Y. Satoh. Can spatiotemporal 3d cnns retrace the history of 2d cnns and imagenet? In *The IEEE Conference on Computer Vision and Pattern Recognition (CVPR)*, 2018.
- [8] Y. Hua, R. Shi, P. Wang, and S. Ge. Learning patch-channel correspondence for interpretable face forgery detection. *IEEE Transactions on Image Processing*, 32:1668–1680, 2023.
- [9] M. Kowalski. Faceswap. <https://github.com/MarekKowalski/FaceSwap/>, 2020.
- [10] L. Li, J. Bao, H. Yang, D. Chen, and F. Wen. Faceshifter: Towards high fidelity and occlusion aware face swapping. *arXiv preprint arXiv:1912.13457*, 2019.
- [11] L. Li, J. Bao, T. Zhang, H. Yang, D. Chen, F. Wen, and B. Guo. Face x-ray for more general face forgery detection. *arXiv preprint arXiv:1912.13458*, 2019.
- [12] Y. Li and S. Lyu. Exposing deepfake videos by detecting face warping artifacts, 2018.
- [13] Y. Li, X. Yang, P. Sun, H. Qi, and S. Lyu. Celeb-df: A new dataset for deepfake forensics. *arXiv preprint arXiv:1909.12962*, 2019.
- [14] I. Masi, A. Killekar, R. M. Mascarenhas, S. P. Gurudatt, and W. AbdAlmageed. Two-branch recurrent network for isolating deepfakes in videos. In *European Conference on Computer Vision*, pages 667–684. Springer, 2020.
- [15] H. H. Nguyen, F. Fang, J. Yamagishi, and I. Echizen. Multi-task learning for detecting and segmenting manipulated facial images and videos. *arXiv preprint arXiv:1906.06876*, 2019.
- [16] A. Rossler, D. Cozzolino, L. Verdoliva, C. Riess, J. Thies, and M. Nießner. Faceforensics++: Learning to detect manipulated facial images. In *Proceedings of the IEEE International Conference on Computer Vision*, pages 1–11, 2019.
- [17] E. Sabir, J. Cheng, A. Jaiswal, W. AbdAlmageed, I. Masi, and P. Natarajan. Recurrent convolutional strategies for face manipulation detection in videos. *Interfaces (GUI)*, 3:1.
- [18] F. Schroff, D. Kalenichenko, and J. Philbin. Facenet: A unified embedding for face recognition and clustering. In *Proceedings of the IEEE conference on computer vision and pattern recognition*, pages 815–823, 2015.
- [19] K. Shiohara and T. Yamasaki. Detecting deepfakes with self-blended images. In *Proceedings of the IEEE/CVF Conference on Computer Vision and Pattern Recognition*, pages 18720–18729, 2022.
- [20] K. Sun, T. Yao, S. Chen, S. Ding, J. Li, and R. Ji. Dual contrastive learning for general face forgery detection. In *Proceedings of the AAAI Conference on Artificial Intelligence*, volume 36, pages 2316–2324, 2022.
- [21] J. Thies, M. Zollhöfer, and M. Nießner. Deferred neural rendering: Image synthesis using neural textures. *ACM Transactions on Graphics (TOG)*, 38(4):1–12, 2019.
- [22] J. Thies, M. Zollhofer, M. Stamminger, C. Theobalt, and M. Nießner. Face2face: Real-time face capture and reenactment of rgb videos. In *Proceedings of the IEEE conference on computer vision and pattern recognition*, pages 2387–2395, 2016.
- [23] D. Tran, H. Wang, L. Torresani, J. Ray, Y. LeCun, and M. Paluri. A closer look at spatiotemporal convolutions for action recognition. In *Proceedings of the IEEE conference on Computer Vision and Pattern Recognition*, pages 6450–6459, 2018.
- [24] H. Zhao, W. Zhou, D. Chen, T. Wei, W. Zhang, and N. Yu. Multi-attentional deepfake detection. In *Proceedings of the IEEE/CVF Conference on Computer Vision and Pattern Recognition*, pages 2185–2194,

- 2021.
- [25] Y. Zheng, J. Bao, D. Chen, M. Zeng, and F. Wen. Exploring temporal coherence for more general video face forgery detection. In *Proceedings of the IEEE/CVF International Conference on Computer Vision*, pages 15044–15054, 2021.